Spin reorientation induced by a very high magnetic field in domain-structured $YFeO_3$ films: Emergence of perpendicular anisotropy

J. Scola,* W. Noun, E. Popova, A. Fouchet, Y. Dumont, and N. Keller
Groupe d'Étude de la Matière Condensée (GEMaC), CNRS-UVSQ, 45 Avenue des États-Unis, 78035 Versailles Cedex, France

P. Lejay
Institut Néel, CNRS–Université Joseph Fourier, Grenoble, France

I. Sheikin and A. Demuer
Grenoble High Magnetic Field Laboratory, CNRS, 38042 Grenoble Cedex 9, France

A. Pautrat
Laboratoire CRISMAT, UMR 6508 du CNRS, ENSICAEN et Université de Caen, 6 Bd. Maréchal Juin, 14050 Caen, France
(Received 27 November 2009; revised manuscript received 19 February 2010; published 13 May 2010)

We report experiments on the static magnetic properties of $YFeO_3$ under magnetic fields up to 28 T. We studied an untwined single crystal, a sintered powder and a film of $YFeO_3$ epitaxially grown by pulsed laser deposition. We proved the relevance of a little used technique, the torque magnetometry, for investigating films having Dzyaloshinsky-Moriya interaction under very high fields. A dedicated framework for analyzing the torque signal in this particular case is also given. We proposed an original model proposed to explain the irreversibility based on the comparison of the morphologies of an experimental study made on purpose. One of the consequences of the particular morphology of films is that the net magnetic moment of the film can be permanently set perpendicular to the substrate plane, giving rise to an effective perpendicular magnetic anisotropy with a coercive field as high as 3 T at room temperature.

DOI: 10.1103/PhysRevB.81.174409 PACS number(s): 75.50.Gg, 75.47.Lx, 75.30.Gw, 75.70.−i

I. INTRODUCTION

Yttrium orthoferrite $YFeO_3$, like all rare-earth orthoferrites, has a distorted perovskite structure (space group $D2h$-16-*Pbnm*). Its low symmetry combined with spin-orbit coupling gives rise to antisymmetric exchange interactions as described by Dzyaloshinsky and Moriya,[1,5] in addition to the antiferromagnetic (AFM) exchange interaction [T_N=648 K (Ref. 8)]. This interaction referred to as Dzyaloshinsky-Moriya (DM) is responsible for the canting angle (a few milliradian[4]) between the two antiferromagnetic sublattices and makes the compound a weak ferromagnet.

We investigate the potentiality of using orthoferrites as a magnetic element in multilayers. The property of interest here is the field-driven spin reorientation (SR) that takes place in $YFeO_3$:[3] as the magnetic field is applied along the antiferromagnetic axis, the weak ferromagnetic moment (WFM) resulting from the canting progressively aligns with the field thus reflecting the rotation of the antiferromagnetic axis from the [100] direction (Γ_4 configuration as denoted in Ref. 9) to the [001] direction at 7.4 T (Γ_2 configuration). SR in orthoferrite is at the origin of a recent breakthrough in ultrafast spin manipulation.[14,15] The epitaxial growth of films of orthoferrites could lead to novel ultrafast devices. Most of the existing studies on films focused on the growth, crystallographic and morphologic aspect, with the aim of using it as exchange bias element for metallic spin valves.[7] Little is known yet on the consequences of the domain-structured morphology on their magnetic properties. The first study of the magnetic properties of films of $YFeO_3$ and other orthoferrites grown on quartz substrate were reported by Schmool *et al.*[6] They observed a static response that stacks two distinct contributions although the films were epitaxially grown and do not have secondary phases. More particularly, they reported a coercive field much higher than in bulk single crystal and ascribed it to the polycrystalinity of their films. Epitaxial films of orthoferrite were later grown on MgO substrates.[13]

In the following, we will first present the static magnetization of an untwined single crystal used as a reference for the rest of the study. Second, we will consider the existence of the DM interaction in the film, in spite of the strain induced by the substrate. To end, we focus on the extrinsic interactions arising from the oriented crystallographic domain structure of the film. For this, we will proceed by direct measurements of the films magnetic properties and by comparison with similar measurements performed on a sintered powder and an untwined bulk single crystal.

II. SAMPLES

A. Films

Our films were grown by pulsed laser deposition (laser Nb:YAG, λ=355 nm) on (100)-$SrTiO_3$ (STO) substrate (cubic a_{STO}=3.905 Å). They are epitaxial and do not have secondary phases. The thickness of the films measured by profilometry is 900 nm and their surface roughness measured by atomic force microscopy is 3 nm rms at the scale of 1 μm. $YFeO_3$ is a distorted perovskite with an orthorhombic structure (*Pbnm* space group). In the bulk, the refined lattice constants are: a=5.2818 Å, b=5.5953 Å, and

 ©2010 The American Physical Society

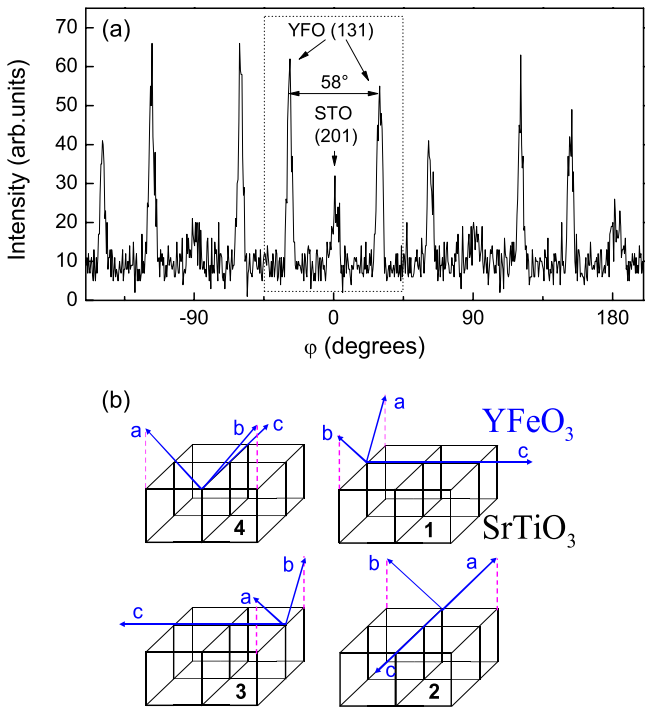

FIG. 1. (Color online) (a) X-ray φ-scan pattern for $YFeO_3$ film grown on STO substrate. The dashed box designates one diffraction pattern that is repeated four times by 90° φ rotations: the (131) peaks are shifted by ±29° around the (201) STO peak. (b) Scheme of the epitaxial growth and the four crystallographic orientations with respect to the $SrTiO_3$ substrate.

c=7.6054 Å. From x-ray (θ–2θ) diffraction the out-of-plane lattice parameter is 0.3796 nm. It is compatible with two possible epitaxial relations: $([001]_{YFO}\|[100]_{STO}$ and $[110]_{YFO}\|[001]_{STO})$ on the one hand and $([100]_{YFO}\|[110]_{STO}$ and $[001]_{YFO}\|[001]_{STO})$ on the other hand. The associated lattice mismatches estimated from bulk lattice parameters are −2.5% and +4.4%, respectively. This first argument in favor of the first possibility is confirmed by the x-ray asymmetrical reflections. Figure 1(a) shows a φ scan where the (201) planes of the substrate are in diffraction conditions at 0°, 90°, 180°, and 270° reflecting the fourfold symmetry expected for the cubic symmetry of STO. In theses conditions, the (131) planes of the film can be in Bragg diffraction condition for the first epitaxial relation and none in the second. The observed eight peaks originating from the film [Fig. 1(a)] rules out the second possibility. The (131) diffraction peaks of $YFeO_3$ are expected to be shifted by $\Delta\varphi$= +28 degrees from the (201) of the substrate. The experimental shift value (+29°) is in good agreement with the theoretical one. In each pattern [dashed box in Fig. 1(a)], the second film peak is observed at $-\Delta\varphi$, coming from the $YFeO_3$ domain rotated by 180°. The film exhibits a fourfold symmetry in the plane although it is orthorhombic. This indicates the presence of four domains rotated by 90° in the plane. Finally, the x-ray experiments output the following morphology of the film: the c axis of $YFeO_3$ is along one of the substrate axis and **a** and **b** are 45° out of the substrate plane; this yields four possible orientations of **c** along the in-plane axes of the substrate [Fig. 1(b)].

Both the epitaxial relation and the morphology have been observed in orthoferrite grown on (100)-STO, for instance, in Lanthanum orthoferrite.[7] We will assume that the domain size in $YFeO_3$ films is the same as in $LaFeO_3$, i.e., a few tens of nanometers.

Each film was cut to supply 5×5 mm^2 and 1×1 mm^2 samples for superconducting quantum interference device (SQUID) and torque experiments, respectively. The presented results were reproduced several times in the same film and also in other films with similar growth conditions.

B. Bulk single crystal

A bulk single crystal was grown using the floating-zone technique in a mirror furnace under air at ambient pressure. X-rays powder-diffraction measurements were carried out on crushed single crystal mixed with pure silicon as standard. The crystal was cut along the crystallographic faces into a $1.90\times1.96\times1.99$ mm^3 cube and a $200\times100\times40$ μm^3 nearly cuboid sample for vibrating sample magnetometer and torque magnetometer, respectively.

C. Sintered powder

High-purity (5N) powders of Fe_2O_3 and Y_2O_3 were mixed, pressed into pellets and sintered according to classical ceramic processing method. The final compound does not contain secondary phases as revealed by x-ray diffraction.

III. EXPERIMENTAL

A. Magnetization

The magnetometer measures the projection of the magnetization along the direction of the applied field. As mentioned above, we model the magnetic response of the thin film by adding the contribution of the four domains, that is,

$$m = \sum_{i=1,\ldots,4} p_i \mathbf{m}_i(\mathbf{H}_i) \cdot \frac{\mathbf{H}}{H}, \tag{1}$$

$\mathbf{m}_i$ being the magnetization of the ith domains, $\mathbf{H}_i$ the magnetic field expressed in a coordinate system $(\mathbf{e_a},\mathbf{e_b},\mathbf{e_c})$ based on the crystallographic axes (considered as orthogonal) of the considered domain, and p_i is the volumic proportion of each domain, with $\Sigma_{i=1,\ldots,4}p_i=1$. The volumic distribution has *a priori* no reason to be nonuniform.

Due to the weakness of magnetic moment in the film, the high sensitivity of the SQUID is required. Since the measured signal is dominated by the diamagnetic response of the STO substrate, the linear dependence of the film magnetization with H (if any) cannot be distinguished with the substrate contribution. Therefore, the linear component of the SQUID magnetization was estimated from the backward branches of the hysteresis cycles and subtracted to the presented data. Blanked data points correspond to spurious measurements of the SQUID when the overall magnetization (film+substrate) crosses the zero line. We report no magnetic influence of the substrate on the films.

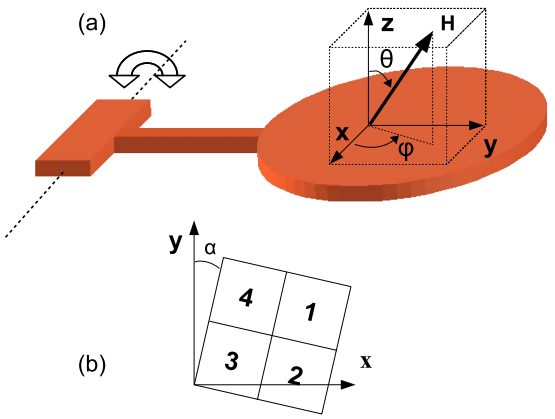

FIG. 2. (Color online) (a) Scheme of the experiment and angles notations. In all experiments, $\varphi=3\pi/2$. (b) Definition of the angle α accounting for the small misalignment of the in-plane film axes with respect to the experiment coordinate system. The numbers refer to the four types of crystallographic domains.

B. Magnetic torque

Magnetization measurements were supplemented by the magnetic torque magnetometry which informs about the magnetization components orthogonal to the applied field and enables measurements at very high magnetic fields (up to 28 T). The samples were rigidly glued on CuBe cantilevers. The small deflections of the cantilever caused by the magnetic coupling of the sample with the applied field ($\mathbf{T}=\mathbf{m}\times\mathbf{H}$) were detected by a high-resolution capacitance bridge. In the experimental configuration, the setup outputs the x component of $\mathbf{T}$ as schemed in Fig. 2(a).

The output signal is proportional to

$$T_x = m_y H_z - m_z H_y \tag{2}$$

with $m_j=\Sigma_{i=1,\ldots,4} p_i \mathbf{m}_i\cdot\mathbf{e}_j$ $(j=y,z)$, $H_y=\sin\varphi\sin\theta$, $H_z=\cos\theta$, and $\varphi=3\pi/2$ in our experimental configuration. We take into account a mechanical misalignment angle α of the substrate axes with respect to the experiment coordinate system [Fig. 2(b)]. Consequently, the relevant components of the film magnetization are

$$\begin{aligned} m_y = {} & p_1\left(\frac{\sqrt{2}}{2}\alpha m_a^{(1)} - \frac{\sqrt{2}}{2}\alpha m_b^{(1)} + m_c^{(1)}\right) + p_3\left(-\frac{\sqrt{2}}{2}\alpha m_a^{(3)}\right. \\ & \left. + \frac{\sqrt{2}}{2}\alpha m_b^{(3)} - m_c^{(3)}\right) + p_2\left(\frac{\sqrt{2}}{2}m_a^{(2)} - \frac{\sqrt{2}}{2}m_b^{(2)} - \alpha m_c^{(2)}\right) \\ & + p_4\left(-\frac{\sqrt{2}}{2}m_a^{(4)} + \frac{\sqrt{2}}{2}m_b^{(4)} + \alpha m_c^{(4)}\right), \end{aligned}$$

$$m_z = \sum_{i=1,\ldots,4} p_i\left(\frac{\sqrt{2}}{2}\alpha m_a^{(i)} + \frac{\sqrt{2}}{2}\alpha m_b^{(i)}\right), \tag{3}$$

where $m_k^{(i)}$ is the magnetization component along the k axis, in the ith type of domains. The orientation of $\mathbf{H}$ in type-i domain is

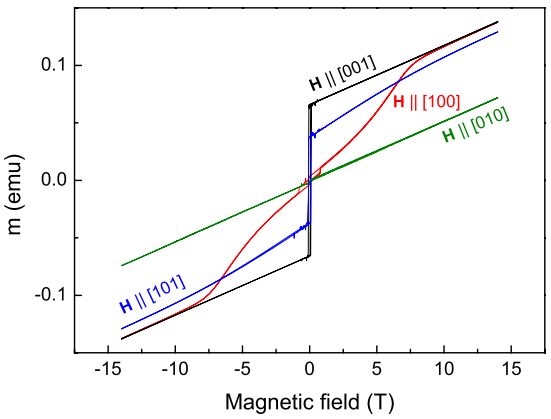

FIG. 3. (Color online) Magnetization of the bulk sample along [100], [010], [001], and [101] directions.

$$\mathbf{H}_{[hk\ell]}^{(i)} \equiv H\frac{h\mathbf{e}_\mathbf{a}^{(i)} + k\mathbf{e}_\mathbf{b}^{(i)} + \ell\mathbf{e}_\mathbf{c}^{(i)}}{\sqrt{h^2+k^2+\ell^2}}; \quad \mathbf{e}_\mathbf{a} = \frac{\mathbf{a}}{a}, \ldots . \tag{4}$$

For sake of clarity, the torque results will be presented divided by the magnetic field and we will consider the quantity

$$\vartheta \equiv T_x/|H|. \tag{5}$$

The absolute value expresses the symmetry with respect to the field polarity. For the same purpose, the trigonometric functions will always be developed to the first order of α and β to simplify the expressions. All measurements were performed at the temperature of 300 K to avoid differential thermal expansion between the film and the substrate.

IV. RESULTS

A. Single-crystal reference

The Fig. 3 shows the magnetization of the macroscopic single crystal for different orientations of the magnetic field. The effect of the magnetic field applied along the direction of the net moment resulting from the canting ($\mathbf{H}\|[001]$) is to increase the canting angle resulting in a linear and reversible variation in the magnetization with the field. As the polarity of the magnetic field is switched, the net moment reverses with a coercive field of about 0.1 T. The spin configuration is Γ_4 for any field. When the field is applied along the AFM axis ($\mathbf{H}\|[100]$), the moment rotates from the [001] direction (null signal) toward the direction of the field yielding a progressive increase of the magnetization along the [100] axis. Above 7.5 T the magnetization curve coincides with that obtained for $\mathbf{H}$ along the canting direction revealing that the SR is complete, i.e., the initial spin configuration has rotated by 90°. The spin configuration is then Γ_2. For $\mathbf{H}\|[010]$, the sample response is linear. It must be noticed that apart from the SR region, the slopes of the three curves are equal. This means that the transverse susceptibility in $YFeO_3$ is isotropic in the plane orthogonal to the AFM axis at room temperature. When the field is applied out of the [001] direction, the irreversibility at low field can be explained by the hysteretic reversal of the m_c component of the WFM due to the mechanical misalignment of the sample. This reproduces the

results of Jacobs *et al.*[3] and shows in addition that the SR is fully reversible.

Also shown is the response of the sample to a field applied along the [101] direction. The WFM reverses at low field and under higher fields, it slightly rotates out of the [001] direction. From all these results, one can draw a global picture of the magnetic interactions in $YFeO_3$ that yield a WFM in an effective anisotropy (a hard and a very hard directions, respectively, [100] and [010]) to which is added a *linear* term coming from the transverse AFM susceptibility.

B. On the existence of antisymmetric exchange in thin film

The lattice mismatch between the film and the substrate induces a strain which is likely to distort the crystallographic structure of $YFeO_3$. Owing to the major importance of the crystal symmetry in this interaction, the antisymmetric exchange may not take place in thin film. The cubic substrate may increase the symmetry of the film, e.g., by making the a and b lattice parameters equal. In our case, the relatively large thickness of the films suggests that the strain induced by the substrate is completely relaxed in most of the film. This assumption is confirmed by the x-ray diffraction results that show a very good agreement of the lattice parameters between the film and single crystals. However, in absence of a direct measurement of the local film symmetry (e.g., by transmission electron microscopy), magnetization will serve to evidence the existence of Dzyaloshinsky-Moriya interaction in films. Magnetization cycles for three different orientations of the applied field with respect to the film are presented in Figs. 4. It should be kept in mind that only the nonlinear dependence with H is presented.

The common points between these three curves are (i) a steep variation below 0.1 T, (ii) an S-shaped at higher field, and (iii) an irreversibility field above 5.5 T. All three features are characteristics of the magnetization cycles in the sintered sample (Fig. 5). The jumps reflect the reversal at low field of the grains having the field mainly along the [001] direction and the S shape arises from the combination of partial SR occurring in grains with a nonzero projection of the field along the [100] direction. The discrepancies between the sintered sample and the film as well as the field orientation dependence in the film are accounted by the fact that the film has only four crystallographic orientations that is not polycrystalline. The magnetization curve is invariant by 90° rotations in the substrate plane, confirming the in-plane fourfold symmetry of the film crystallographic structure observed by x-ray diffraction.

The comparison of the magnetic curves in the film with that of a sintered powder shows that the interactions in bulk $YFeO_3$, and particularly the DM interaction, are preserved in films. The substrate strain is relaxed in such a way that the alteration the antisymmetric exchange interaction is negligible. However, the film's magnetic response cannot be described as a mere addition of individual domains. The irreversibility of the magnetization curve clearly shows that interdomain coupling intervenes. In the following, we will study the static coupling through the magnetic response

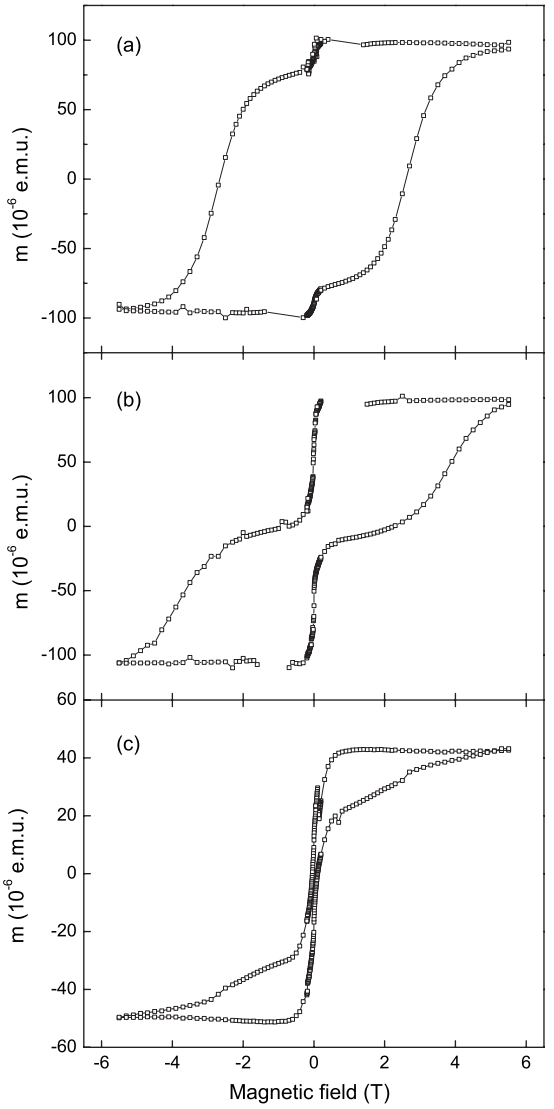

FIG. 4. Magnetization measured by SQUID of the thin film for different orientations of the applied field: (a) perpendicular to the film, (b) 45° out-of-the-film plane, and (c) in-plane.

(magnetization and torque experiment) of the film under high magnetic fields and for different field orientations. The coupling will be considered as a perturbation to the simple model of independent domains which will be given by direct measurements on the single crystal in the appropriate field orientations.

C. Angular dependence of the magnetic response in film

1. Perpendicular field experiment

First, the magnetic field was applied along the normal of the film plane: $\mathbf{H}=H\mathbf{e_z}$. Given the epitaxy relation [see Fig. 1(b)], $\mathbf{H}$ is applied in the [110] direction in every domain ($H_{1,\ldots,4}=H_{[110]}$). In this configuration, the projection of the magnetic moment of the film along the field direction is

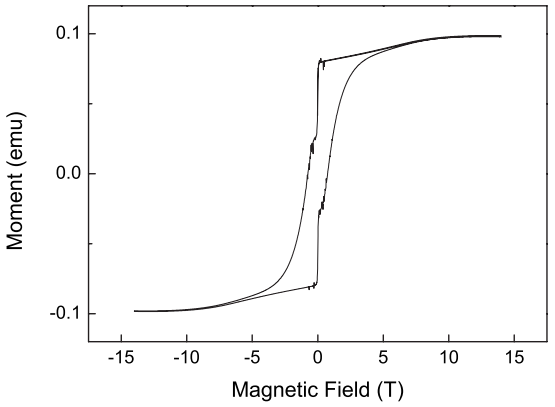

FIG. 5. Magnetization of a $YFeO_3$ sintered powder. The linear term (8.75 10^{-3} emu/T) was subtracted for sake of comparison with films.

$$m(\theta = -\beta) = \frac{\sqrt{2}}{2}[m_a(\mathbf{H}_{[110]}) + m_b(\mathbf{H}_{[110]})]. \quad (6)$$

Since m_b is linear with H, it cannot be distinguished from the diamagnetic response of the substrate and will be neglected in the following. Thus, the SQUID experiment outputs

$$m(\theta = -\beta) = \frac{\sqrt{2}}{2} m_a(\mathbf{H}_{[110]}). \quad (7)$$

A minor magnetization cycle is reproduced in Fig. 4(a). The upward-field branches exhibit the characteristic S shape of the SR, similar to that of the bulk curve for **H** applied along **a** (Fig. 3). The backward branches are flat plateaus that reflect the remanence of the magnetic moment in its direction after the SR. The plateaus are broken by a relatively sharp drop below 0.1 T.

The high-field magnetization was investigated by torque magnetometry. Since the torque vanishes as the field is collinear with a symmetry axis of the magnetic structure, the field was misaligned by a small angle β. Here, $\beta = 6°$ and this value will be the same in all our experiments. In perpendicular field $\theta = -\beta$ and $\varphi = 3\pi/2$. For this orientation, the expression of ϑ can be obtained from Eqs. (2) and (3)

$$\vartheta(\theta = -\beta) \approx p_1 m_c^{(1)}(\mathbf{H}_{[110]}) + p_3 m_c^{(3)}(\mathbf{H}_{[110]}) - \frac{\sqrt{2}}{2}\beta \sum_{i=1,\ldots,4} p_i [m_a^{(i)}(\mathbf{H}_{[110]}) + m_b^{(i)}(\mathbf{H}_{[110]})]. \quad (8)$$

In this configuration, the observed quantity is a combination of the in plane moment in type-1 and type-3 domains and the total out-of-plane moment, weighted by the misalignment β. The first term should vanish at high field when the SR has taken place ($m_c = 0$ in the Γ_2 configuration). The magnetic torque measured in perpendicular field is reproduced in Fig. 6.

a. Initial magnetization. Before the first application of the magnetic field, the magnetization is along **c** of the four domain types (Γ_4 spin configuration); the WFM is close to zero and so is ϑ. As the field increases the magnetic torque decreases down to negative values, reflecting the increase (decrease) in the m_a (respectively, m_c): the WFM moments rotates around **b** from [001] to [100]. This reorientation spans up to the maximum field. Interestingly, as the field is reduced, ϑ decreases even further showing the system is not yet in a reversible state despite the applied field of 28 T.

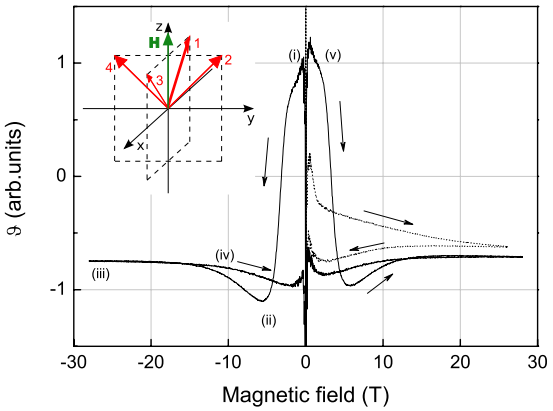

FIG. 6. (Color online) Magnetic torque of the thin film in perpendicular applied field. Dashed line: initial magnetization of the sample and solid line: full magnetization loop. The roman numbers designates the different configurations described in the text. Inset: sketch of the WFM in the four domains at high field.

b. Hysteresis loop. When the field polarity is switched (i) the absolute value ϑ is kept constant but its sign changes indicating that the remanence of the WFM in the [100] direction while H crosses zero (since the torque changes sign when H *or* m does). This confirms the interpretation of the above SQUID experiment. The subsequent path of the magnetic moment during the reorientation can be deduced from the torque curve. Up to $H = 5.5$ T (ii) ϑ falls down to a minimum value that corresponds to the opposite of the low field value, indicating that the moments have completely reversed. The phenomenon spreads over several tesla and corresponds to a progressive reorientation rather than sharp reversal. As the field further increases (iii), ϑ decreases in absolute value. This means that the magnetic moment is reorienting toward the direction of the magnetic field; the SR takes place in two steps: first from [100] to $[\bar{1}00]$, then to an given direction in the (001) plane, toward the applied field direction. (iv) Interestingly, the moment is blocked again in the latter reorientation as the field decreases: the moment is still tilted away from the a axis at $H = 5.5$ T. The small decrease in ϑ at low field may be associated with the partial drop in the magnetization curve but the large difference of field sweep rate between the two experiments prevents from concluding on this. After the second inversion of the field polarity (v) ϑ switches sign again, confirming the remanence of WFM in the [100] direction. This shows that the SR is irreversible: once the moments are driven to the a direction they stick in their new position.

2. Oblique field experiments

In this part, the field is applied along the a axis of type-4

domains. The corresponding magnetic cycle is shown in Fig. 4(b). The cycle can be decomposed into two additive contributions. On the one hand, the moment reversal of the net moment like in the single-crystal sample for $\mathbf{H}\|\mathbf{c}$. On the other hand, a hysteretical S-shape curve similar to that of Fig. 4(a).

According to Eq. (1), the projection of the magnetic moment along the field direction is given in Eq. (9)

$$m\left(\theta=\frac{\pi}{4}-\beta\right)=p_1\left[\frac{1}{2}m_a^{(1)}(\mathbf{H}_{[11\bar{1}]})+\frac{1}{2}m_b^{(1)}(\mathbf{H}_{[11\bar{1}]})+\frac{\sqrt{2}}{2}m_c^{(1)}(\mathbf{H}_{[11\bar{1}]})\right]+p_3\left[\frac{1}{2}m_a^{(3)}(\mathbf{H}_{[111]})+\frac{1}{2}m_b^{(3)}(\mathbf{H}_{[111]})+\frac{\sqrt{2}}{2}m_c^{(3)}(\mathbf{H}_{[111]})\right]$$
$$+p_4m_a^{(4)}(\mathbf{H}_{[100]})+p_2[m_a^{(2)}(\mathbf{H}_{[010]})+m_b^{(2)}(\mathbf{H}_{[010]})]. \quad (9)$$

It can be seen from this expression that the moment reversal is due to the domains in which **H** is mainly along the **c** (types 1 and 3 here) and the smooth reorientation to the 4-type domains where the spin configuration has been once driven to Γ_2 and where a 180° SR takes place between [100] and $[\bar{1}00]$. Very little can be known about magnetization in type-2 domains by SQUID magnetometry.

The expression of ϑ for this field orientation can be obtained like previously

$$\vartheta\left(\theta=\frac{\pi}{4}-\beta\right)=p_1\left[\frac{1}{2}(1+\alpha-\beta)m_a^{(1)}(\mathbf{H}_{[11\bar{1}]})+\frac{1}{2}(1-\alpha-\beta)m_b^{(1)}(\mathbf{H}_{[11\bar{1}]})+\frac{\sqrt{2}}{2}(1+\beta)m_c^{(1)}(\mathbf{H}_{[11\bar{1}]})\right]+p_3\left[\frac{1}{2}(1-\alpha-\beta)m_a^{(3)}\right.$$
$$\left.\times(\mathbf{H}_{[111]})+\frac{1}{2}(1+\alpha-\beta)m_b^{(3)}(\mathbf{H}_{[111]})-\frac{\sqrt{2}}{2}(1+\beta)m_c^{(3)}(\mathbf{H}_{[111]})\right]+p_4\left[-\beta m_a^{(4)}(\mathbf{H}_{[100]})+m_b^{(4)}(\mathbf{H}_{[100]})+\frac{\sqrt{2}}{2}\alpha m_c^{(4)}(\mathbf{H}_{[100]})\right]$$
$$+p_2\left[m_a^{(2)}(\mathbf{H}_{[010]})-\beta m_b^{(2)}(\mathbf{H}_{[010]})-\frac{\sqrt{2}}{2}\alpha m_c^{(2)}(\mathbf{H}_{[010]})\right]. \quad (10)$$

The sign of the torque is a good guide to analyze the results. The magnetization measurement [Fig. 4(b)] showed that the magnetic moment inside the type-1 and type-3 domains are mainly along **c**. If each domain were isolated, the type-1 (respectively, type-3) domains WFM would tend to be tilted away from the [001] direction toward the $[11\bar{1}]$ (respectively, [111]) field and the two first terms of Eq. (10) would give a negative contribution to the torque and they would tend to vanish at high field as the WFM aligns with the applied field. Besides, Fig. 4(b) showed that the magnetization of type-4 domains undergoes a rotation between [100] and $[\bar{1}00]$ directions around 6 T, thus contributing positively below 6 T and negatively at higher field. It should be noticed that the misalignment factor implies this term to be negligible with respect to the others. It is obvious that these two phenomena are not enough to account for the measured torque. This indicates that the magnetization of type-2 domains contributes significantly to ϑ. For the fourth term of Eq. (10) to be positive and prevail in ϑ, the WFM of type-2 domains must point in the [100] direction. In that case, ϑ is dominated by type-2 domains magnetization where the WFM is aligned with the *a* axis and undergo a 180° SR like in the perpendicular field configuration. The orientation of the WFM in the plane orthogonal to the magnetic field is a rather unexpected result that could not have been detected by the SQUID technique. Once the reorientation is completed, the torque slowly drifts down from a positive value as *H* increases further. This slight decrease in ϑ reflects the alignment of the WFM toward the field direction. It must be noticed that this second step is reversible while it was not the case in perpendicular field.

When the magnetic polarity is changed, ϑ keeps its absolute value but changes sign, showing that the observed WFM in type-2 domains remains in the [100] direction (it can be inferred that the moments in type-4 domains are frozen too). More than 6 T in the opposite polarity are needed to fully reorient the net moment in the opposite direction. The magnetic response to an oblique field is analog as for a perpendicular field, apart from the fact that the reorientation takes place in only half the sample. In the other half, where the field is mainly along [001], the response is analog to that of an isolated single crystal.

3. In-plane field experiments

We now consider the magnetic field applied along the axis of the substrates, that is along the *c* axis of two domains and along the *ab* diagonal of the two others. Let **H** be in the direction of the *c* axis of type-3 domains when $H>0$. According to Eq. (1), the magnetic signal measured by the SQUID magnetometer can be expressed by

$$m\left(\theta=\frac{\pi}{2}-\beta\right)=-p_1[m_c^{(1)}(-\mathbf{H}_{[\mathbf{001}]})+p_3m_c^{(3)}(\mathbf{H}_{[\mathbf{001}]})$$
$$+p_2\left\{\frac{\sqrt{2}}{2}[-m_a^{(2)}(\mathbf{H}_{[\bar{1}\bar{1}\mathbf{0}]})+m_b^{(2)}(\mathbf{H}_{[\bar{1}\bar{1}\mathbf{0}]})\right\}$$
$$+p_4\left\{\frac{\sqrt{2}}{2}[+m_a^{(4)}(\mathbf{H}_{[1\bar{1}\mathbf{0}]})-m_b^{(4)}(\mathbf{H}_{[1\bar{1}\mathbf{0}]})\right\}. \quad (11)$$

In Fig. 4(c) is presented a minor magnetization cycle for the magnetic field applied parallel to the thin film. Like previously, the sharp drop of the magnetization that occurs below 0.1 T comes from the first two terms of Eq. (11). The progressive increase at higher field corresponds to a partial SR in type-2 and type-4 described by the last two terms of Eq. (11). As in the other field orientations, the SR is irreversible and several tesla in the opposite polarity are needed to reverse the spin configuration.

The high-field magnetization was measured by the torque technique. In our notations [Fig. 1(b)], the in-plane field is defined by $\theta = \pi/2 - \beta$. The $\vartheta(H)$ curve is presented in Fig. 4(c). The field was first increased up to 28 T in the positive polarization, then decreased to 0. The maximum field was limited to 5.5 T in negative polarization for comparison with SQUID experiment (full cycles were performed on three other samples and output symmetric patterns with respect to the field polarity).

The expression of the output signal is obtained using Eqs. (2) and (3)

$$\vartheta\left(\theta = \frac{\pi}{2} - \beta\right) = p_1 \beta m_c^{(1)}(-\mathbf{H}_{[001]}) - p_3 \beta m_c^{(3)}(\mathbf{H}_{[001]}) + p_2\left[\frac{\sqrt{2}}{2}(1+\beta)m_a^{(2)}(-\mathbf{H}_{[1\bar{1}0]}) + \frac{\sqrt{2}}{2}(1-\beta)m_b^{(2)} \times(-\mathbf{H}_{[1\bar{1}0]})\right] + p_4\left[\frac{\sqrt{2}}{2}(1-\beta)m_a^{(4)}(\mathbf{H}_{[1\bar{1}0]}) + \frac{\sqrt{2}}{2}(1+\beta)m_b^{(4)}(\mathbf{H}_{[1\bar{1}0]})\right]. \quad (12)$$

From the isolated single crystal reference, the WFM of uneven type domains is expected to be collinear with **H** and that of the even domains should lie in the [001] plane. Then, the first two terms are negative constant and the positive contribution to ϑ must correspond to the last two terms. Let $\cos\delta^{(2,4)}\mathbf{a} + \sin\delta^{(2,4)}\mathbf{b}$ be the unit vector of the WFM in these domains. If one assumes that for a strong enough field each of the two vectors were mainly directed toward the direction of **H** (i.e., to the left on the inset of the Fig. 8), the measured torque signal would be expressed as $\vartheta(\theta = \frac{\pi}{2} - \beta) = -\frac{1}{2}\beta - \frac{\sqrt{2}}{4}\beta(\cos\delta + \sin\delta)$ which is negative. Although intuitive, this possibility is clearly ruled out by the experiment. Instead, we suggest an alternative hypothesis in coherence with the observed results. Given the importance of memory effects in our system, the interpretation of its magnetic behavior should be guided by its history. In the present case, the torque experiment in parallel field was made immediately after the oblique field one. As a consequence, the state of the system at the beginning of the experiment in parallel field was that depicted in the inset of Fig. 7. Figure 8 shows that between 3 and 10 T, ϑ evolves toward the opposite of its initial value. This result suggests that the effect of the applied field is to reverse the WFM in type-2 and type-4 domains while preserving their relative orientation. As in the oblique field configuration, the WFM in type-2 that is kept mainly orthogonal to the applied field in any case. This scenario is sketched in the inset of the Fig. 8. Once the magnetic pattern is reversed, a further increase in the magnetic field up to 28 T leads to a small decrease in ϑ. This corresponds to the progressive tilt of the film net moment toward the direction of the applied field.

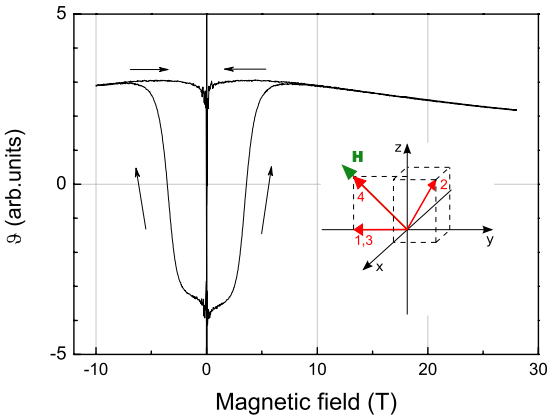

FIG. 7. (Color online) Magnetic torque of the thin film with the field applied 45° out-of-the-substrate plane (see text). Inset: sketch of the WFM in the four domains at high field.

In order to compare with the SQUID experiments, a torque minor cycle ($|H| < 5.5$ T) is presented in the Fig. 8. Given the value of ϑ is dominated by the type-2 domains WFM, the minor cycle corresponds to the beginning of the [100]-to-[$\bar{1}$00] reversal that takes place in this domains. When the field is reversed at 5.5 T, the plateau shape of the downward branch of ϑ reveals that the magnetic configuration is frozen down to $H = 0$ T. This confirms the irreversibility of the [100]-to-[$\bar{1}$00] magnetic reversal as suggested by the SQUID experiments.

V. DISCUSSION

Combined together, these six experiments bring a global description of the static magnetization in each crystallographic domain as a function of the applied field. (i) The magnetization of the domains having **H** mostly along the [001] direction (type-1 and type-3) reverses along the c axis

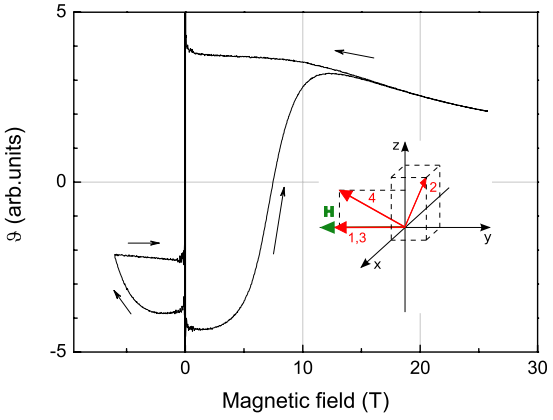

FIG. 8. (Color online) Magnetic torque measured in the thin film with the magnetic field applied in the substrate plane (see text). Inset: sketch of the WFM in the four domains at high field.

at low field (typically 0.1 T) and eventually tilt away from the *c* axis toward the direction of **H** as the field further increases. This is the behavior of an isolated single crystal. (ii) Once the SR from Γ_4 to Γ_2 has been driven by the applied field in a given domain, its spin configuration remains in Γ_2 at $H=0$ T. When several tesla are applied in the opposite polarity, the WFM rotates by 180° around the [010] axis between [100] and [$\bar{1}$00].

In the discussion of the coupling mechanism, we will suppose that the magnetic domains coincide with the crystal domains. This simplification is justified by the very high speed of the magnetic domain walls in $YFeO_3$.[2]

The most dramatic consequence of the coupling is the remanence of the out-of-plane magnetization. We attribute it to an exchange coupling between the magnetization in neighbor domains added to the intrinsic effective field of $YFeO_3$. When the SR occurs in a given domain, the out-of-plane component of its magnetization creates a bias field within its neighbors thus facilitating the reorientation there. In the case of the perpendicular field experiment, once all domains are in Γ_2 configuration the system is globally self-biased and the configuration is kept even at $H=0$. The intensity of the coupling has to be compared to the 7 T required to induce the SR in an isolated single crystal. Also, several tesla in the opposite polarization are needed to overcome the self-biasing field and to reverse the magnetization. Such a strong coupling can stem from the high magnetic moment of iron sites (the magnetic moment per iron ion can be estimated from the Fig. 3 and Ref. 4 to be around $3.2\mu_B$). Similarly to ferrimagnets, low-dimensional effects and surface spin disorder may perturbate the canted AFM order leading to strong magnetic moment at the boundary between crystallographic domains.[10] This picture is coherent with NMR investigations in single crystals that suggest that strong deviation from the equilibrium spin configuration order that the AFM order can occur in 90° magnetic domain walls.[11] However, it must be stressed that due to their particular morphology films hardly compare to single crystals so that little can be known about the magnetic configuration at the crystallographic boundaries in films without direct observations.

The experiments show that the magnetization of Γ_4 configuration domains always reverses at low field with the same coercive field as an isolated single crystal regardless of the neighboring magnetization. The situation occurs in domains where **H** is mainly along the WFM spontaneous direction ([001]): the Γ_4 configuration is thus favored and the WFM is less likely to rotate under its neighbors bias fields. Furthermore, the WFM results from the canting of two sublattices and can therefore reverse by cancellation instead of rotation. This makes the reversal process easier and regardless of the anisotropies and couplings. As for the small sharp drop in the magnetization cycles in perpendicular field [Fig. 4(a)], where the in-plane component of **H** is negligible, it can be ascribed to weakly coupled domains (e.g., at the edges of the sample).

From the technological point of view, $YFeO_3$ fulfills numerous requirements for a suitable development of applications. Its high magnetic ordering temperature makes it very stable at room temperature, it is appropriate for multilayers because of its low interdiffusion and it is oxidation resistant. We showed here that a particular morphology in epitaxial films leads to an out-of-plane magnetization with a very strong effective magnetic anisotropy. Perpendicular magnetized films have potential applications in magnetic random access memory [using, e.g., giant magnetoresistant (GMR) multilayers] and magneto-optic devices. Strong perpendicular anisotropies can arise from surface or interface effects. Ultrathin Co films with perpendicular anisotropy have coercive fields up to 1.2 kOe and the saturation magnetization is around 100 kA/m.[16] Coercive fields up to 2 kOe have been obtained by surface engineering of Fe-Pd films.[12] In $Mn_{1-x}Ga_x$, where the perpendicular anisotropy is of magnetocrystalline origin rather than induced by extrinsic effects, coercive fields as high as 6.3 kOe have been obtained and the saturation magnetization of 460 kA/m.[17] Our films of $YFeO_3$ are quite competitive with these systems: from Fig. 4(a), the ferromagnetic moment in the film that is about 5 kA/m and the coercive field can be estimated from Fig. 6 around 33 kOe. With these characteristics $YFeO_3$ films offer a new and very promising solution for applications, and particularly as exchange bias element in a perpendicular anisotropy GMR.

VI. CONCLUSION

We reported a study of the static magnetic properties in untwined single crystal, sintered powder, and epitaxial films of $YFeO_3$ under high magnetic fields. We paid particular attention to the field-driven spin reorientation occurring around 7 T. We reproduced former experiments on single crystals and provided extra results: the reversal of the weak ferromagnetic moment resulting from the canting reverses very sharply and the coercive field is about 0.1 T. Also shown is the fact that the field-driven spin reorientation is completely reversible. By measuring the magnetization with **H** along the three crystallographic axes, the anisotropy of the plane orthogonal to the AFM axis was demonstrated. Our films of $YFeO_3$ epitaxially grown by pulsed laser deposition exhibit the same magnetic features as bulk samples of $YFeO_3$.

The comparison between the polycrystal, the film with oriented crystallographic domains and the single crystal, revealed that the spin reorientation is reversible only in single crystal. A very strong coupling between crystallographic domains exists in the sintered powder and the film and it gives rise to the remanence of the reoriented state (Γ_2). The particular morphology of the film leads to subtle history effects and particularly to a permanent out-of-plane magnetic moment when a perpendicular field is applied. Then, more than 5 T in the opposite polarity are needed to fully reverse the magnetization. It is worth noticing that the out-of-plane remanent magnetization with high coercive field makes $YFeO_3$ films very attractive candidates for exchange biasing elements in magnetic multilayers.

*joseph.scola@uvsq.fr

[1] I. Dzyaloshinsky, J. Phys. Chem. Solids **4**, 241 (1958).
[2] T. Ikuta and R. Shimizu, J. Phys. D **7**, 2386 (1974).
[3] I. S. Jacobs, H. F. Burne, and L. M. Levinson, J. Appl. Phys. **42**, 1631 (1971).
[4] H. Lütgemeier, H. Bohn, and M. Brajczewska, J. Magn. Magn. Mater. **21**, 289 (1980).
[5] T. Moriya, Phys. Rev. **120**, 91 (1960).
[6] D. S. Schmool, N. Keller, M. Guyot, R. Krishnan, and M. Tessier, J. Appl. Phys. **86**, 5712 (1999).
[7] J. W. Seo, E. E. Fullerton, F. Nolting, A. Scholl, J. Fompeyrine, and J.-P. Locquet, J. Phys.: Condens. Matter **20**, 264014 (2008).
[8] D. Treves, Phys. Rev. **125**, 1843 (1962).
[9] R. M. White, R. J. Nemanich, and C. Herring, Phys. Rev. B **25**, 1822 (1982).
[10] X. Batlle and A. Labarta, J. Phys. D **35**, R15 (2002).
[11] S. Nadolski and H. Szymczak, J. Magn. Magn. Mater. **21**, 167 (1980).
[12] C. Clavero, J. R. Skuza, Y. Choi, D. Haskel, J. M. Garcia-Martin, A. Cebollada, and R. A. Lukaszew, Appl. Phys. Lett. **92**, 162502 (2008).
[13] Y. Dumont, M. Vedpathak, N. Keller, M. Tessier, A. Tromson-Carli, and M. Guyot, J. Cryst. Growth **244**, 274 (2002).
[14] A. V. Kimel, A. Kirilyuk, A. Tsvetkov, R. V. Pisarev, and T. Rasing, Nature (London) **429**, 850 (2004).
[15] A. V. Kimel, A. Kirilyuk, P. A. Usachev, R. V. Pisarev, A. M. Balbashov, and T. Rasing, Nature (London) **435**, 655 (2005).
[16] A. Kirilyuk, J. Ferré, V. Grolier, J. P. Jamet, and D. Renard, J. Magn. Magn. Mater. **171**, 45 (1997).
[17] K. M. Krishnan, Appl. Phys. Lett. **61**, 2365 (1992).